*Materials Research*. 2014; 17(3): 542-549
DOI: http://dx.doi.org/10.1590/S1516-14392014005000050


# Synthesis and Characterization of $Fe_3O_4$ Nanoparticles with Perspectives in Biomedical Applications

***Javier Bustamante Mamani*[a]*, *Lionel Fernel Gamarra*[a,b,c], *Giancarlo Espósito de Souza Brito*[d]**

[a]*Hospital Israelita Albert Einstein – HIAE, São Paulo, SP, Brazil*
[b]*Departamento de Neurologia e Neurocirurgia,*
*Universidade Federal de São Paulo – UNIFESP, São Paulo, SP, Brazil*
[c]*Faculdade de Ciências Médicas da Santa Casa de São Paulo – FCMSCSP, São Paulo, SP, Brazil*
[d]*Departamento de Física Aplicada, Instituto de Física – IF,*
*Universidade de São Paulo – USP, São Paulo, SP, Brazil*

Received: February 27, 2013; Revised: December 5, 2013

Nowadays the use of magnetic nanoparticles (MNP) in medical applications has exceeded expectations. In molecular imaging, MNP based on iron oxide coated with appropriated materials have several applications *in vitro* and *in vivo* studies. For applications in nanobiotechnology these MNP must present some characteristics such as size smaller than 100 nanometers, high magnetization values, among others. Therefore the MNP have physical and chemical properties that are specific to certain studies which must be characterized for quality control of the nanostructured material. This study presents the synthesis and characterization of MNP of magnetite ($Fe_3O_4$) dispersible in water with perspectives in a wide range of biomedical applications. The characterization of the colloidal suspension based on MNP stated that the average diameter is (12.6±0.2) nm determined by Transmission Electron Microscopy where the MNP have the crystalline phase of magnetite ($Fe_3O_4$) that was identified by Diffraction X-ray and confirmed by Mössbauer Spectroscopy. The blocking temperature of (89±1) K, $Fe_3O_4$ MNP property, was determined from magnetic measurements based on the Zero Field Cooled and Field Cooled methods. The hysteresis loops were measured at different temperatures below and above blocking temperature. The magnetometry determined that the MNP showed superparamagnetic behavior confirmed by ferromagnetic resonance.

**Keywords:** *nanoparticles, iron oxide, synthesis, characterization, magnetite*

## 1. Introduction

The synthesis of magnetic nanoparticles (MNP) has received great interest in recent years because of new physical and chemical properties of materials at nanoscale. Based on their mesoscopic physical, chemical, thermal and mechanical properties, and in conjunction with control of size, composition and morphology of growth, the synthesis of MNP lead to a wide range of specific technological applications[1-4].

Among crystal polymorphs of iron (III) known, magnetite ($Fe_3O_4$) is a promising candidate for its biocompatibility and biodegradable activity[5,6]. Thus, iron oxide MNP with crystalline phase corresponding to magnetite appears as an important nanomaterial for various biomedical applications such as: (i) cellular therapy as cell labeling, targeting, and as a tool for cell-biology research to separate and purify cell populations, (ii) tissue repair; (iii) drug delivery, (iv) magnetic resonance imaging (MRI), (v) hyperthermia, (vi) magnetofection, among other[7-9]. In clinical applications, it is desirable MNP with sizes between 10 and 200 nm, because MNP larger than 200 nm can be filtered by the human spleen, and MNP smaller than 10 nm can be removed by renal clearance[10]. The usefulness of MNP in medical applications is mainly related to the coating material, which are biocompatible, nontoxic and biodegradable. Among the commercial products based on MNP, Endorem® and Lumirem® are used as contrast agents in MRI to the liver and intestine, respectively.

Several synthesis processes are used in the development of MNP. For this reason, the conditions of synthesis are crucial to determine the physicochemical properties of MNP such as concentration and pH of the solution as well as the mode of heat treatment used[11,12]. The most important methods described in the literature to prepare MNP, which are suitable for biomedical applications[13-16], are: co-precipitation, microemulsions polyol process, high temperature decomposition of organic precursors, assisted sonochemical, electrochemical methods and sol-gel process. It is important for biomedical applications, to know the synthesis process of the nanomaterial – which needs to be dispersed in water – and also, the study of biocompatibility and toxicity that must possess adequate characteristics for such applications. In the case of iron oxide MNP coated with biocompatible material determining the crystal phase, the average diameter and the magnetic property are important, which can be measured using several techniques.

*e-mail: javierbm@einstein.br

This paper presents a synthesis route to prepar MNP as well as the morphological, structural and magnetic characterization of the material synthesized to control quality of these MNP that are presented as promising particles in biomedical applications. Morphological characterization was performed using the technique of transmission electron microscopy (TEM). The structural characterization was conducted using the technique of X-ray diffraction (XRD) and Mössbauer spectroscopy. The magnetic characterization was done using magnetometry (SQUID) and ferromagnetic resonance (FMR).

## 2. Experimental

### 2.1. *Magnetic fluid preparation*

An alcoholic solution 200 ml of $FeCl2_3.6H_2O$ (Aldrich) 0.25M, in butanol, was prepared and heated under stirring to 90 °C. So, 8 mL of concentrated surfactant nonilpheniletoxilated (Renex 95®), another solution of concentrated ammonia was prepared containing 4% (in volume) of surfactant (Renex 95®).

The ammonia solution was added drop by drop to the iron III solution to promote precipitation of iron oxi-hydroxide. The precipitate was centrifuged and washed with butanol containing 4% (in volume) of surfactant at 90 °C in order to eliminate as possible the ammonium chloride. After five washing cycles, we observed the peptization of the precipitate and formation of 100 mL of true sol. Subsequently, 8 mL of surfactant (Renex 95®) and 10 mL of liquid paraffin (Nujol®) were added to the sol.

The sol was dried at 70 °C under stirring to aid butanol evaporation. After that, a viscous dark liquid was obtained. The viscous dark liquid was dried in a hermetically closed sintering chamber at 250 °C under $N_2$ pressure (2 atm) for half-hour.

After complete the procedure described above, we obtained a black paste. This paste was dispersed in water containing 4% of surfactant (Renex 95®) that formed a magnetic fluid.

### 2.2. *Characterization methods*

The crystalline phase of the redispersible black paste was determined by X-ray diffraction (XRD). The XRD data were collected between $10° < 2\theta < 60°$ using the Cu-Kα radiation filtered by Ni in step scanning mode (0.05° for 10 s).

Mössbauer spectroscopy (MS) measurements were performed at 78 K and 294 K using a constant-acceleration spectrometer in transmission geometry with a $^{57}Co/Rh$ source. To calibrate isomer shifts and velocity scale, we used a foil of α-Fe at 294 K. For magnetic measurements, as-prepared samples were stored in closed containers before quenching the magnetite/carrier mixture below its freezing point (~268 K) at room temperature.

Transmission electronic microscopy (TEM) was employed to check the size distribution of nanoparticles in the magnetic fluid. The magnetic fluid was dried at 70 °C by water evaporation. Fine powders were aspersed on a cooper grille containing parlodion and charcoal, and examined using a LEO 906E equipment operating at 80 KV.

The nanoparticles size poly-dispersity was analyzed from the TEM micrographies using the image analysis program java ImageJ v 1.33u[17]. Mean diameters were thus obtained by fitting the experimental data with a lognormal distribution function, as suggested by O'Grady and Bradbury[18].

$$f(D_p) = \frac{1}{\sqrt{2\pi}\omega_P D_P} \exp\left( -\frac{\left(\ln D_P - \ln D_P^0\right)^2}{2\omega_P^2} \right) \quad (1)$$

With mean diameter $\langle D_P \rangle = D_P^0 \exp(\omega_P^2/2)$ and $\omega_P$ as the standard deviation around $\ln D_P^0$. The standard deviation of the mean diameter $\sigma_P$ is

$$\sigma_P = D_P^0[\exp(2\omega_P^2) - \exp(\omega_P^2)]^{1/2} \quad (2)$$

A commercial SQUID magnetometer was employed to perform static and dynamic measurements as a function field, temperature and driving frequency. Zero-field-cooled (ZFC) and field-cooled (FC) curves were taken in applied magnetic fields up to 7 T, between 5K and 250 K to avoid melting of the solid matrix (solvent).

We used a ferromagnetic resonance (FMR) to verify the superparamagnetic behavior and to evaluate the nanoparticles geometry. The derivative of the FMR absorption spectrum was obtained using a Brucker X band homodyne spectrometer, model EMX-12 operating at frequency of 9.2GHz and modulated at 100 KHz with a $TE_{102}$ dominant mode cavity. The measurements were carried out at room temperature.

## 3. Results and Discussion

Figure 1 shows the XRD profile of the redispersible powder sample. We could observe a large low crystallinity zone with $2\theta = 30.19°$. Typical diffuse profiles of iron oxide phases are added to the background and can be attributed to maghemite ($\gamma$-$Fe_2O_3$, ICSD Collection Code 79196), magnetite ($Fe_3O_4$, ICSD Collection Code 15840)

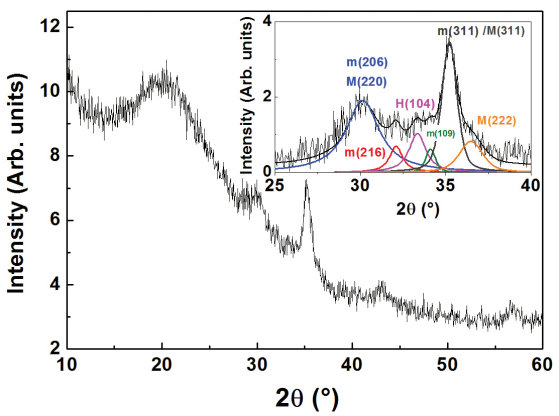


**Figure 1.** Diffractogram of the synthesized sample, the inset shows the possible existence of iron oxides magnetite (M), maghemite (m) and / or hematite (H).

or hematite ($\alpha$-$Fe_2O_3$, ICSD Collection Code 66756) corresponding to small crystalline domains. Following the profile analyses, the background was subtracted and the presence of two intense peaks between 25 and 40 (2θ°) can be noted. In order to access the structural parameters, the $K\alpha_1$-$K\alpha_2$ doublet separation (Rachinger correction) and background corrections were performed by using a pseudo-Voigt function (PVF), in a interactive method of profile fitting by least squares method[19,20]. The peak position and correspondent phase were chosen as initial parameters. The inset of the Figure 1 shows the results of the fit procedure and the result exhibits basically peaks due maghemite phase. On other hand, the XRD results point out to a mixed phase of iron oxide constituted by $Fe^{2+}$ and $Fe^{3+}$ ions.

The structural characterization by XRD of MNP is complex, because the diffractogram shows broad and overlapping diffraction peaks due to finite number of scattering crystalline planes that are causing the positions and shapes of the peaks to vary according to the nanoparticles size, making difficult to interpret the diffractograms. It is important to mention that in the case of existence or coexistence of magnetite, maghemite and / or hematite it is difficult to identify the crystalline phase formed from the techniques of X-ray diffraction, because they do not have obvious structural differences shown in the inset Figure 1, for example, peak M(220) and m(206), and peak M(311) and m(311). Therefore, alternative methods are needed that allow to individualize these oxides, such as Mössbauer spectroscopy technique that allows to perform local measures and sensitive to the vicinity of the chemical elements, thereby allowing a better identification of the phases formed.

For better identification of magnetic phases presented in the synthesized sample we used a Mossbauer spectroscopy, which showed a structure constituted with two different magnetic ions occupying two classes of binding sites in the crystal lattice, tetrahedral (A) and octahedral (B). The room temperature Mossbauer spectra in Figure 2a corresponds to magnetite ($Fe_3O_4$), where all changes in the interactions (AA, AB and BB) are aligned anti-parallel. The behavior ferrimagnetism is because of strong interaction of AB. The favorable antiparallel interaction of A with B induces the parallel ordering of all the spins of A and B and the system is ordered ferrimagnetism.

The room temperature Mossbauer spectra is presented in Figure 2a. The hyperfine parameters for this latter presented in Table 1 agree with those for A and B sites of magnetite. In agreement with the expected superparamagnetic in our sample at T = 78 K, described in Figure 2b, the spectrum showed nearly total magnetic order, although relaxing particles could still be inferred from the curved background. T=4.2 K in Figure 2c the spectra could be fitted with only two magnetically ordered components of hyperfine fields $B_1 = 50.7(4)$ T and $B_2 = 52.9(4)$ T, which correspond to sites A ($Fe^{3+}$ ions) and B ($Fe^{2+}$ $Fe^{3+}$ ions) respectively. Both sites showed nearly null quadrupole splitting QS and intensity ratio B:A ~ 2:1. All these hyperfine parameters are very close to those of bulk magnetite at this temperature, without any indication of finite-size effects. These bulk-like properties are seemingly originated in a well-ordered local structure

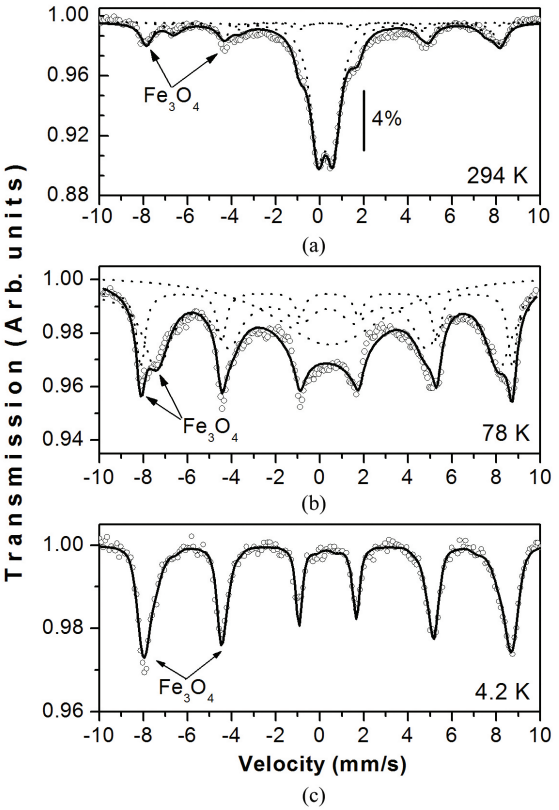


**Figure 2.** Mössbauer spectrum: (a) room temperature, (b) 78 K e (c) 4.2 K.

**Table 1.** Hyperfine parameters.

| T (K) | | $B_{hyp}$ (T) | QS (mm/s) | IS (mm/s) | I (%) |
|---|---|---|---|---|---|
| **294** | A | 49.8(2) | 0.0(1) | 0.32(8) | 53(8) |
| | B | 44.0(2) | 0.0(1) | 0.50(8) | 47(8) |
| **78** | A | 52.3(2) | 0.1(1) | 0.50(8) | 57(11) |
| | B | 48.0(3) | 0.0(1) | 0.52(8) | 43(11) |
| **4.2** | A | 52.9(1) | 0.0(1) | 0.50(8) | 67(3) |
| | B | 50.7(1) | 0.0(1) | 0.52(8) | 36(3) |

within the particles. However, the large spectral linewidth ($\Gamma$=0.7 mm/s) observed in the sample suggests the presence of a second phase.

The literature describes the average diameter calculation of the nanoparticles core by the XRD technique. This type of analysis is based on the diffraction line profile, where the Scherrer[21] method is the most used for its simplicity, which may lead to results with little accuracy associated with the complexity of the diffraction pattern. However, exist more efficient methodologies for this calculation such as the Warren-Averbach modified method[21]. Given the complexity of determining the sample crystal phase of XRD spectrum, this calculation was not performed in our study. Therefore, the TEM technique was chosen to analyze the measurement of average diameter for the synthesized nanoparticles..

As regards the morphological characterization, TEM technique allowed to observe the morphology and distribution of MNP in colloidal suspension after drying by lyophilization of the sample (Figure 3). The size distribution was fitted to a log-normal function from the histogram (see inset of Figure 3) obtained from the micrograph. In setting the average diameter was found $<D_P>$ = 12.6 nm with a typical width $\sigma_P$ = 0.2. The histogram was obtained by the analysis of micrograph (Figure 3) considering more than 700 particles.

The Figure 4 shows magnetization curves taken in zero-field-cooling (ZFC) and field-cooling (FC) modes with $H_{app}$=100 Oe. The sample showed superparamagnetic behavior at room temperature, with blocking transition at

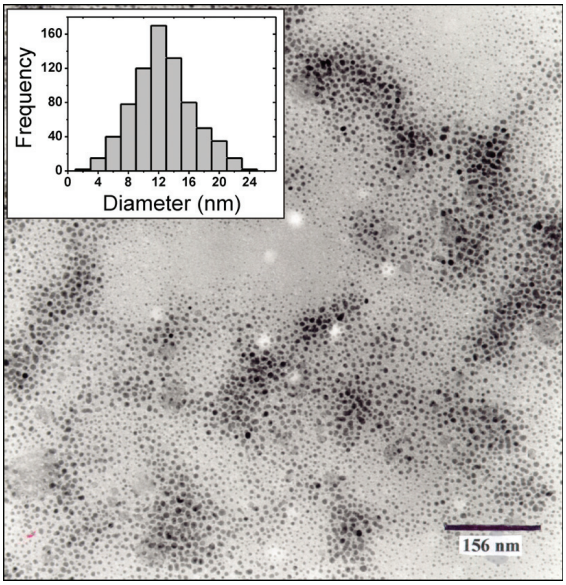


**Figure 3.** Transmission electron micrograph of the synthesized ferrofluid (77500X). The inset shows the histogram of size distribution of MNP which was obtained from TEM data to approximate a log-normal distribution with mean diameter $<D_P>$ = 12.6 nm with typical width $\sigma_P$ = 0.2.

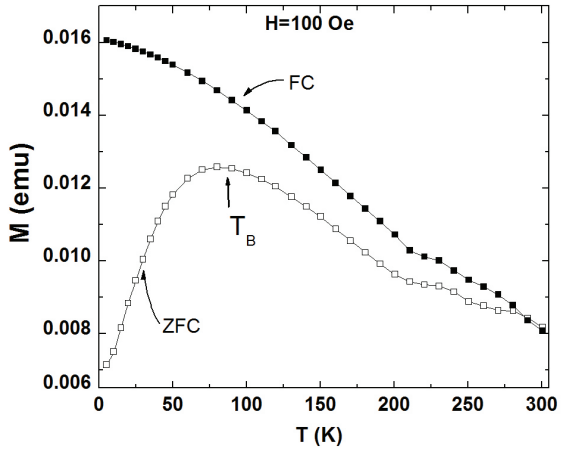


**Figure 4.** Curve fitting ZFC and FC measurements at 100 Oe.

$T_B$ = 89(1) K (H=100 Oe). The lack of overlapping Zero-field- cooled (ZFC) and field-cooled (FC) curves indicated that the largest particles were blocked at 300 K, the highest temperature obtained in our study. The great value of $T_B$ and broader peak of ZFC data were consistent with the average size of MNP and the size distribution.

Figure 5 shows the magnetization versus field plot at temperatures of 150 K (a) and 10 K (b). Figure 5a shows that hysteresis disappeared with a little remanence and coercirvity ($H_c$), indicating the absence as a long range magnetic dipole-dipole interaction among the assemblies of superparamagnetic nanoparticles. When the temperature was decreased to 10 K, the magnetization of the sample increased with a symmetric hysteresis loop, and showed a transition from superparamagnetic to ferromagnetic behavior (Figure 5b).

For $T > T_B$ the coercitivity $H_C$ of the particles is zero within experimental error, whereas below $T_B$ the coercive field increases up to a value $H_C$ = 330(5) Oe at 2 K. This value of $H_C$ is within the (broad) range reported for nanostructured iron oxide nanoparticles. The remanence to saturation ratio $R = M_R/M_S$ measured at 5 K is 0.27, smaller than the theoretically expected 0.5 for randomly oriented grains[22], some studies had proposed that R > 0.5 and R < 0.5 values should be expected for systems with ferro- and antiferromagnetic interactions, respectively. Thus, the presented R = 0.27 value suggests that the interparticle interactions are of antiferromagnetic nature.

Findings of this study shows that Ms of synthesized MNP was lower than the corresponding bulk phase. Studies on the reduction in magnetization in iron oxide nanoparticles ($\gamma$-$Fe_2O_3$, $Fe_3O_4$) had reported that reduction is because of the existence of noncollinear spins at the surface of the nanoparticles[5,23]. Varanda et al.[24] described

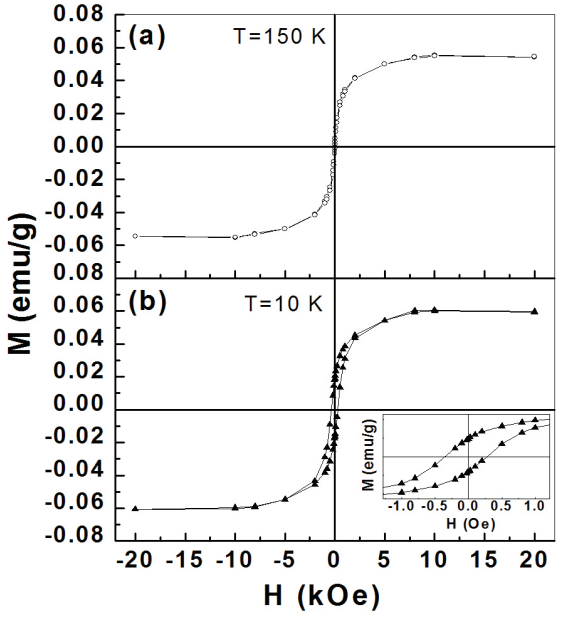


**Figure 5.** Magnetization as a function of magnetic field at temperatures of 150 K (a) and 10 K (b).

a linear correlation between Ms and nanoparticles size suggesting that defects at the nanoparticle surface can influence the magnetic properties[5,24]. The surface curvature of particles was higher for nanoparticles which stimulated disordered crystal orientation on the surface resulting in significantly decreased Ms[5]. The identification of the hard crystalline phase by X-ray diffraction, Figure 1, suggests reduction in the magnetization which is associated with the surface feature of the MNP. This loss of magnetisation depends primarily on the crystalline magnetic anisotropy energy constant, K indicating that magnetization losses are associated with the existence of a magnetically dead layer, ~ 1 nm thick, caused by an asymmetric environment effect on surface atoms[5,25]. The magnetic behavior depends on MNP $T_B$, $T_B$ being dependent on the size of the MNP. MNP with low values of $T_B$ exhibit superparamagnetic properties. For high values of the $T_B$ MNP showed ferromagnetic behavior[10]. For MNP average diameter <30nm the remanence and coercivity are very small so that producing a superparamagnetic behavior of MNP[26]. The values of remanence and coercivity, almost zero, are shown in the hysteresis loops of the nanomaterial. The figure 5 shows that the synthesized MNP has the superparamagnetic property which is a desirable characteristic of a nanomaterial in biomedical applications. Studies show that the MNP coating with non-magnetic materials decrease saturation magnetization values[27,28]. A magnetically ineffective layer on the MNP surface interferes in determining the particle sizes calculated using magnetization data smaller than values calculated from measurements performed by structural techniques such as XRD and TEM morphology[29]. This analysis enabled us to state that MNP with crystallization of the magnetite synthesized under different conditions

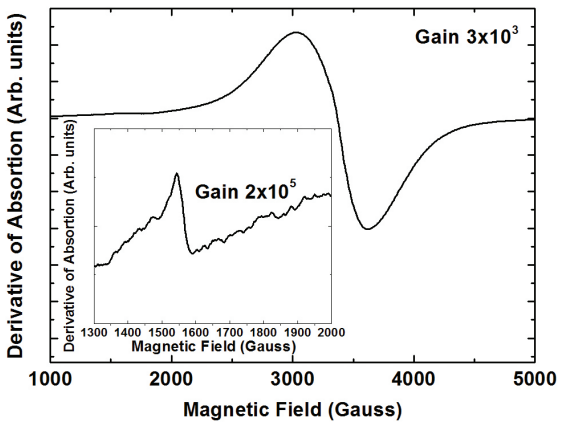


**Figure 6.** FMR spectrum of the synthesized ferrofluid at room temperature. In the inset the resonance is enhanced in g=4.3.

differ from MNP's magnetic properties that are attributed to changes in the structural disorder, the creation of antiphase boundaries or the existence of a magnetically dead layer in the surface of MNP[5,30-32].

The magnetic properties of synthesized MNP in colloidal suspension were also studied by FMR. The FMR spectrum obtained at room temperature of the ferrofluid synthesized (Figure 6) showed two resonance lines whose parameters are shown in Table 2. The main resonance (g=2.0) came from the $Fe^{3+}$ spins interactions, however, such interactions showed a superparamagnetic behavior[33-39] characterized by the presence of clusters. This signal consists of a strong absorption slightly asymmetric, whose large width is attributed to the strong interaction between Fe ions (cluster of clusters of $Fe^{3+}$ ions by a strong exchange interaction). The exchange interaction between spins aligned antiparallel means that a broadening of resonance lines exist and this extension depends on the concentration of iron ions.

A second additional line was observed, but with low intensity, suggesting the presence of traces of $Fe^{3+}$ (g=4.3) in the form of ions isolated trapped between oxygen atoms in sites that could provide local symmetry tetrahedral or octahedral, corresponding to iron paramagnetic. This line, presented by low intensity in the commercial ferrofluid is attributed to the existence of a paramagnetic complex of $Fe^{3+}$ in the sample or the thermal fluctuations of the anisotropy axis of the magnetic particle[33,34].

The analysis of the FMR spectrum obtained at room temperature allows to conclude that the synthesized sample has a superparamagnetic property[40,41] which is required for several applications. We did not perform a detailed analysis of FMR spectrums in the studied sample. It could be made by obtaining spectrums achieved within the temperature range from 4K to room temperature, which allowed the analysis of various parameters typically originated from iron oxide nanoparticles[40,41]. In the FMR analysis as a function of temperature, we could observe that the peak to peak amplitude varied because randomly oriented dispersed ferromagnetic particles the width of absorption line is a monotonic function of temperature. At low temperature, the line width is larger due to the particles dispersion in the direction of the anisotropy field, because as temperature decreases, isotropic magnetic moments are formed and causes a decrease in the line width[40,42].

To determine nanostructured material characteristics, without the need to make a detailed analysis along with the toxicity and biocompatibility tests at biological level, is enough to predict the potential application in molecular imaging and nanomedicine[43]. The biological part was not the objective of this work: however, because of the MNP properties and the character of biocompatible coating, the

**Table 2.** FMR parameters obtained from Figure 6.

| | $H_{res}$ (Gauss) (f=9.428GHz) | $\Delta H_{pp}$ (Gauss) | g-factor |
|---|---|---|---|
| Resonance 1 | 3362 ± 5 | (6.0 ± 0.3)×10² | 2.0030 ± 0.0001 |
| Resonance 2 | 1564.3 ± 0.5 | 47 ± 9 | 4.3044 ± 0.0001 |

possible biomedical applications of the synthesized material are: (i) Because of superparamagnetic character, the sample can be used as a negative contrast agent for weighted images in the transverse relaxation time ($T_2$) in magnetic resonance imaging[44]; (ii) the biocompatible coating and the property of being dispersed in an aqueous medium is essential for biological applications during the intracelular labeling of different cell lineages, for example, tumorigenic cells[45]; (iii) the superparamagnetic characteristic of the nanomaterial is a property that can facilitate the nanoparticles uptake by the cells through the use of an external static magnetic field[46-48]; (iv) in the magneto hyperthermia, where selective thermal ablation of tumor is made using MNP exposed to alternating magnetic field[49,50]; (v) MNP stability in the blood would allow the MNP to be guided or directed through a magnetic field gradient for targets such as tumor tissue, allowing the nanomaterial accumulation in the tumor tissue of interest[47,51].

## 4. Conclusions

A chemical synthesis route was used to produce a ferrofluid-based MNP redispersible in water and different techniques were used to determine the characteristics of synthetized MNP.

This study reveals that MNP have an average diameter (12.6±0.2) nm as evidenced by the TEM technique. XRD showed the crystalline phase of iron oxide could correspond to magnetite, maghemite or hematite, but the characterization by Mössbauer determined the crystalline phase corresponds to magnetite ($Fe_3O_4$). The Mössbauer spectra at T = 294K showed that nanoparticles are in superparamagnetic state. The magnetization measurements showed ZFC and FC transition to the blocking state $T_B = (89 \pm 1)$ K. Measure of magnetization as a function of the field showed a typical behavior of superparamagnetism in material because there were no coercitivity for T>TB the hysteresis cycles. However, when the temperature decreases below the blocking temperature, the magnetization of the sample increases with symmetrical hysteresis loop, showing a transition from superparamagnetic to ferromagnetic behavior. The study by FMR at room temperature showed that the ferrofluid reveals superparamagnetic behavior.

The average diameter of MNP characterized by TEM revealed to be ideal for *in vitro* studies. The crystalline phase of magnetite identified by Mössbauer is the most widely used in biological applications. The property of superparamagnetism determined by magnetometry and FMR allows MNP to be used in the monitoring and tracking of MNP by MRI technique, as well as in the Magneto Hyperthermia technique.

We believe synthetized nanomaterial has a potential for biomedical applications. Nonetheless, it is clear that both *in vitro* and *in vivo* studies are necessary to determine the applicability of this sample.

## Acknowledgments

This work was supported by Instituto Israelita de Ensino e Pesquisa Albert Einstein - IIEPAE, FINEP, CAPES, CNPq and FAPESP.

## References

1. Lin MM, Kim DK, El Haj AJ and Dobson J. Development of Superparamagnetic Iron Oxide Nanoparticles (SPIONS) for Translation to Clinical Applications. *IEEE transactions on Nanobioscience*. 2008; 7(4):298-305. http://dx.doi.org/10.1109/TNB.2008.2011864
2. Teja AS and Koh PY. Synthesis, properties, and applications of magnetic iron oxide nanoparticles. *Progress in Crystal Growth and Characterization of Materials*. 2009; 55(1-2):22-45. http://dx.doi.org/10.1016/j.pcrysgrow.2008.08.003
3. Kim J, Piao Y and Hyeon T. Multifunctional nanostructured materials for multimodal imaging, and simultaneous imaging and therapy. *Chemical Society Reviews*. 2009; 38(2):372-390. http://dx.doi.org/10.1039/b709883a
4. Shubayev VI, Pisanic Ii TR and Jin S. Magnetic nanoparticles for theragnostics. *Article Advanced Drug Delivery Reviews*. 2009; 61(6):467-477. http://dx.doi.org/10.1016/j.addr.2009.03.007
5. Gupta AK and Gupta M. Synthesis and surface engineering of iron oxide nanoparticles for biomedical applications. *Biomaterials*. 2005; 26(18):3995-4021. http://dx.doi.org/10.1016/j.biomaterials.2004.10.012
6. Xie J, Xu CJ, Xu ZC, Hou YL, Young KL, Wang SX et al. Linking Hydrophilic Macromolecules to Monodisperse Magnetite ($Fe_3O_4$) Nanoparticles via Trichloro-s-triazine. *Chemistry of Materials*. 2006; 18(23):5401-5403. http://dx.doi.org/10.1021/cm061793c
7. Arbab AS, Bashaw LA, Miller BR, Jordan EK, Lewis BK, Kalish H et al. Characterization of Biophysical and Metabolic Properties of Cells Labeled with Superparamagnetic Iron Oxide Nanoparticles and Transfection Agent for Cellular MR Imaging. *Radiology*. 2003; 229(3):838-846. http://dx.doi.org/10.1148/radiol.2293021215
8. Pankhurst QA, Connolly J, Jones SK and Dobson J. Applications of magnetic nanoparticles in biomedicine. *Journal of Physics D: Applied Physics*. 2003; 36:R167. http://dx.doi.org/10.1088/0022-3727/36/13/201
9. Sensenig R, Sapir Y, MacDonald C, Cohen S and Polyak B. Magnetic nanoparticle-based approaches to locally target therapy and enhance tissue regeneration *in vivo*. *Nanomedicine*. 2012; 7(9):1425-1442. http://dx.doi.org/10.2217/nnm.12.109
10. Chatterjee J, Haik Y and Chen Ch-J. Size dependent magnetic properties of iron oxide nanoparticles. *Journal of Magnetism and Magnetic Materials*. 2003; 257(1):113-118. http://dx.doi.org/10.1016/S0304-8853(02)01066-1
11. Tang DP, Yuan R and Chai YQ. Direct Electrochemical Immunoassay Based on Immobilization of Protein-Magnetic Nanoparticle Composites on to Magnetic Electrode Surfaces by Sterically Enhanced Magnetic Field Force. *Biotechnology Letters*. 2006; 28(8):559-565. http://dx.doi.org/10.1007/s10529-006-0017-4
12. Zboril R, Mashlan M and Petridis D. Iron(III) Oxides from Thermal ProcessesSynthesis, Structural and Magnetic Properties, Mössbauer Spectroscopy Characterization, and Applications. *Chemistry of Material*. 2002; 14(3):969-982. http://dx.doi.org/10.1021/cm0111074
13. Wu W, He Q and Jiang Ch. Magnetic Iron Oxide Nanoparticles: Synthesis and Surface Functionalization Strategies. *Nanoscale Research Letters*. 2008; 3:397-415. http://dx.doi.org/10.1007/s11671-008-9174-9
14. Laurent S, Forge D, Port M, Roch A, Robic C, Elst LV et al. Magnetic Iron Oxide Nanoparticles: Synthesis, Stabilization, Vectorization, Physicochemical Characterizations, and

Biological Applications. *Chemical Reviews*. 2008; 108 (6):2064-2110. http://dx.doi.org/10.1021/cr068445e

15. Mamani JB, Costa-Filho AJ, Cornejo DR, Vieira ED and Gamarra LF. Synthesis and characterization of magnetite nanoparticles coated with lauric acid. *Materials Characterization*. 2013; 81:28-36. http://dx.doi.org/10.1016/j.matchar.2013.04.001
16. Brinker CJ and Scherrer GW. Sol-gel Science: The Physics of Chemistry of Sol-gel Processing. Academic Press, New York; 1990.
17. Rasvand W. *Image Processing and Analysis in Java*; 2004. Available from: <http://rsb.info.nih.gov/ij>. Acces in: 18/12/2012.
18. O'Grady K and Bradbury A. Particle size analysis in ferrofluids. *Journal of Magnetism and Magnetic Materials*. 1983; 39(1-2):91-94. http://dx.doi.org/10.1016/0304-8853(83)90407-9
19. Klug HP and Alexander L. X Ray Procedures for Polycrystalline and Amorfous Materials. 2nd ed. USA: John Wiley; 1974.
20. Brito GES. *Evolução Estrutural e Microestrutural Durante a Secagem e Sinterização de Géis a Base de Óxido de Estanho.* [Doctoral Thesis]. Brazil: Instituto de Química de Araraquara, Universidade Estadual Paulista Júlio de Mesquista Filho; 1997.
21. Dorofeev GA, Streletskii AN, Povstugar IV, Protasov AV and Elsukov EP. Determination of nanoparticle sizes by X-ray diffraction. *Colloid Journal*. 2012; 74(6):675-685. http://dx.doi.org/10.1134/S1061933X12060051
22. Stoner EC and Wohlfarth EP. A Mechanism of Magnetic Hysteresis in Heterogeneous Alloys. *Philosophical Transactions of the Royal Society A*. 1948; 240(826):599-642. http://dx.doi.org/10.1109/TMAG.1991.1183750
23. Coey J. Noncollinear spin arrangement in ultrafine ferromagnetic crystallites. *Physical Review Letters.* 1971; 27:1140-3. http://dx.doi.org/10.1103/PhysRevLett.27.1140
24. Varanda LC, Jafelicci P Jr, O'Grady K, González-Carreño T, Morales MP, Muñoz T et al. Structural and magnetic transformation of monodispersed iron oxide particles in a reducing atmosphere. *Journal of Applied Physics.* 2002; 92(4):2079. http://dx.doi.org/10.1063/1.1496124
25. Sato T, Iijima T, Sekin M, Inagaki N. Magneticproperties of ultrafine ferrite particles. *Journal of Magnetism and Magnetic Materials* 1987; 65:252. http://dx.doi.org/10.1016/0304-8853(87)90044-8
26. Unsoy G, Yalcin S, Khodadust R, Gunduz G, Gunduz U. Synthesis optimization and characterization of chitosan-coated iron oxide nanoparticles produced for biomedical applications. *Journal of Nanoparticle Research.* 2012; 14: 964. http://dx.doi.org/10.1007/s11051-012-0964-8
27. Gomez-Lopera SA, Plaza RC, Delgado AV. Synthesis and characterization of spherical magnetite/biodegradable polymer composite particles. *Journal of Colloid and Interface Science.* 2001; 240(1):40-7. http://dx.doi.org/10.1006/jcis.2001.7579
28. Voit W, Kim DK, Zapka W, Muhammed M, Rao KV. Magnetic behavior of coated superparamagnetic iron oxide nanoparticles in ferrofluids. *Materials Research Society.* 2001; 676:Y7.8 .1-6. http://dx.doi.org/10.1557/PROC-676-Y7.8
29. Bradbury A, Menear S, O'Grady K, Chantrell RW. Magnetic size determination for interacting fine particle systems. *IEEE Transactions on Magnetics.* 1984; 20(5):1846-8. http://dx.doi.org/10.1109/TMAG.1984.1063338
30. Taylor AP, Barry JC, Webb RI. Structural and morphological anomalies in magnetosomes: possible biogenicorigin for magnetite in ALH84001. *Journal of Microscopy.* 2001; 201(1):84. http://dx.doi.org/10.1046/j.1365-2818.2001.00760.x
31. Zhou WL, Wang K-Y, O'Connor CJ, Tang J. Granular growth of Fe3O4 thin films and its antiphase boundaries prepared by pulsed laser deposition. *Journal of Applied Physics*. 2001; 89(11): 7398-400. http://dx.doi.org/10.1063/1.1358831
32. Kim DK, Zhang Y, Voit W, Rao KV, Kehr J, Bjelke B, Muhammed M. Superparamagnetic iron oxide nanoparticles for bio-medical applications. *Scripta Materialia* 2001; 44:1713-7. http://dx.doi.org/10.1016/S1359-6462(01)00870-3
33. Sharma VK and Waldner F. Superparamagnetic and ferrimagnetic resonance of ultrafine $Fe_2O_4$ particles in ferrofluids. *Journal of Applied Physics*. 1977; 48(10):4298-4302. http://dx.doi.org/10.1063/1.323418
34. Raikher YL and Stepanov VI. Ferromagnetic resonance in a suspension of single-domain particles. *Physical Review B*. 1994; 50(9):6250-6259. http://dx.doi.org/10.1103/PhysRevB.50.6250
35. Morais PC, Lara MCF and Skeff Neto K. Electron spin resonance in superparamagnetic particles dispersed in a non-magnetic matrix. *Philosophical Magazine Letters*. 1987; 55(4):181-183. http://dx.doi.org/10.1080/09500838708207553
36. Nagata K and Ishihara A. ESR of ultrafine magnetic particles. *Journal of Magnetism and Magnetic Materials*. 1992; 104-107(3):1571-1573. http://dx.doi.org/10.1016/0304-8853(92)91459-7
37. Sastry MD, Babu Y, Goyal PS, Mehta RV, Upadhyay RV and Srinivas D. Electron magnetic resonance of ferrofluids: Evidence for anisotropic resonance at 77 K in samples cooled in a magnetic field. *Journal of Magnetism and Magnetic Materials*. 1995; 149(1-2):64-66. http://dx.doi.org/10.1016/0304-8853(95)00339-8
38. Berger R, Bissey JC, Kliava J, Daubric H and Estournes C. Temperature dependence of superparamagnetic resonance of iron oxide nanoparticles. *Journal of Magnetism and Magnetic Materials*. 2001; 234(3):535-544. http://dx.doi.org/10.1016/S0304-8853(01)00347-X
39. Hseih CT, Huang WL and Lue JT. The change from paramagnetic resonance to ferromagnetic resonance for iron nanoparticles made by the sol-gel method. *Journal of Physics and Chemistry of Solids*. 2002; 63(5):733-741. http://dx.doi.org/10.1016/S0022-3697(01)00222-0
40. Gamarra LF, Pontuschka WM, Mamani JB, Cornejo DR, Oliveira TR, Vieira, ED et al. Magnetic characterization by SQUID and FMR of a biocompatible ferrofluid based on $Fe_3O_4$. *Journal of Physics: Condensed Matter*. 2009; 21:115104. http://dx.doi.org/10.1088/0953-8984/21/11/11510
41. Gamarra LF, Mamani JB, Carneiro SM, Fabris JD, Ferreira RV, Domingues RZ et al. Characterization of Superparamagnetic Iron Oxide Coated with Silicone Used as Contrast Agent for Magnetic Resonance Image for the Gastrointestinal Tract. *Journal of Nanoscience and Nanotechnology*. 2010; 10:1153-1158. http://dx.doi.org/10.1166/jnn.2010.1843
42. Kinnari P, Upadhyay RV and Mehta RV. Magnetic properties of Fe-Zn ferrite substituted ferrofluids. *Journal of Magnetism and Magnetic Materials*. 2002; 252:35-38. http://dx.doi.org/10.1016/S0304-8853(02)00652-2
43. Chen X, Lv H, Ye M, Wang S, Ni E, Zeng F et al. Novel superparamagnetic iron oxide nanoparticles for tumor embolization application: preparation, characterization and double targeting. *International Journal of Pharmaceutics*. 2012; 426(1-2):248-55. http://dx.doi.org/10.1016/j.ijpharm.2012.01.043

44. Mamani JB, Malheiros JM, Cardoso EF, Tannús A, Silveira PH and Gamarra LF. *In vivo* magnetic resonance imaging tracking of C6 glioma cells labeled with superparamagnetic iron oxide nanoparticles. *Einstein (Sao Paulo)*. 2012; 10(2):164-70. http://dx.doi.org/10.1590/S1679-45082012000200009

45. Mamani JB, Pavon LF, Miyaki LA, Sibov TT, Rossan F, Silveira PH et al. Intracellular labeling and quantification process by magnetic resonance imaging using iron oxide magnetic nanoparticles in rat C6 glioma cell line. *Einstein (Sao Paulo)*. 2012; 10(2):216-221. http://dx.doi.org/10.1590/S1679-45082012000200016

46. Smith CA, de la Fuente J, Pelaz B, Furlani EP, Mullin M and Berry CC. The effect of static magnetic fields and tat peptides on cellular and nuclear uptake of magnetic nanoparticles. *Biomaterials*. 2010; 31(15):4392-400. http://dx.doi.org/10.1016/j.biomaterials.2010.01.096

47. Landázuri N, Tong S, Suo J, Joseph G, Weiss D, Sutcliffe DJ et al. Magnetic Targeting of Human Mesenchymal Stem Cells with Internalized Superparamagnetic Iron Oxide Nanoparticles. *Small*. 2013. http://dx.doi.org/10.1002/smll.201300570

48. Chertok B, David AE, Huang Y and Yang VC. Glioma selectivity of magnetically targeted nanoparticles: a role of abnormal tumor hydrodynamics. *Journal of Controlled Release*. 2007; 122(3):315-23. http://dx.doi.org/10.1016/j.jconrel.2007.05.030

49. Jordan A, Scholz R, Maier-Hauff K, van Landeghem FK, Waldoefner N, Teichgraeber U et al. The effect of thermotherapy using magnetic nanoparticles on rat malignant glioma. *Journal of Neuro-Oncology*. 2006; 78(1):7-14. http://dx.doi.org/10.1007/s11060-005-9059-z

50. Silva AC, Oliveira TR, Mamani JB, Malheiros SM, Malavolta L, Pavon LF et al. Application of hyperthermia induced by superparamagnetic iron oxide nanoparticles in glioma treatment. *International Journal of Nanomedicine*. 2011; 6:591-603. http://dx.doi.org/10.2147/IJN.S14737

51. Chertok B, David AE and Yang VC. Brain tumor targeting of magnetic nanoparticles for potential drug delivery: Effect of administration route and mangetic field topography. *Journal of Controlled Release*. 2011; 155(3):393-399. http://dx.doi.org/10.1016/j.jconrel.2011.06.033